Exceptional Fatigue Life and ductility of New Liquid Healing Hot Isostatic Pressing Especially Tailored for Additive Manufactured Aluminum Alloys

Julie Gheysen[a], David Tingaud[b], Julie Villanova[c], Azziz Hocini[b] and Aude Simar[a]*

[a] Université catholique de Louvain, Institute of Mechanics, Materials and Civil Engineering (iMMC), 1348 Louvain-la-Neuve, Belgium.

[b] Université Sorbonne Paris Nord, Laboratoire des Sciences des Procédés et des Matériaux, UPR 3407, CNRS, 93430 Villetaneuse, France.

[c] ESRF - The European Synchrotron, CS 40220, 38043, Grenoble Cedex 9, France.

*corresponding author : julie.gheysen@epfl.ch and present address: Ecole Polytechnoque Fédérale de Lausanne, Faculté des Sciences et Techniques de l'Ingénieur (STI), 1015 Lausanne, Switzerland.

Abstract:

Porosity and hot cracking still hinder the introduction of new additive manufactured alloys on the market, which requires high reliability. Hot Isostatic Pressing (HIP) is thus commonly applied to close these defects. Although HIP showed promising results as post-treatment on steel and titanium alloys, it is detrimental on aluminum alloys. Liquid assisted healing is thus applied during HIP to not only compress the pores, leading to stress concentration defects but to completely heal them. An Al-Mg alloy was manufactured as a proof-of-concept and X-ray nano-holo-tomography highlighted the healing of almost all the defects, even a 80 µm diameter pore, during liquid assisted HIP. This leads to the substantial increase of the fracture strain by a factor 3 without strength loss and an exceptional increase in fatigue life up to a factor 100. This healing HIP treatment is promising for post-treatment of other Al alloys but also as in-service healing treatment.

Keywords: hot isostatic pressing (HIP), liquid assisted healing, aluminum alloy, laser powder bed fusion (LPBF), fatigue life.

Graphical abstract:

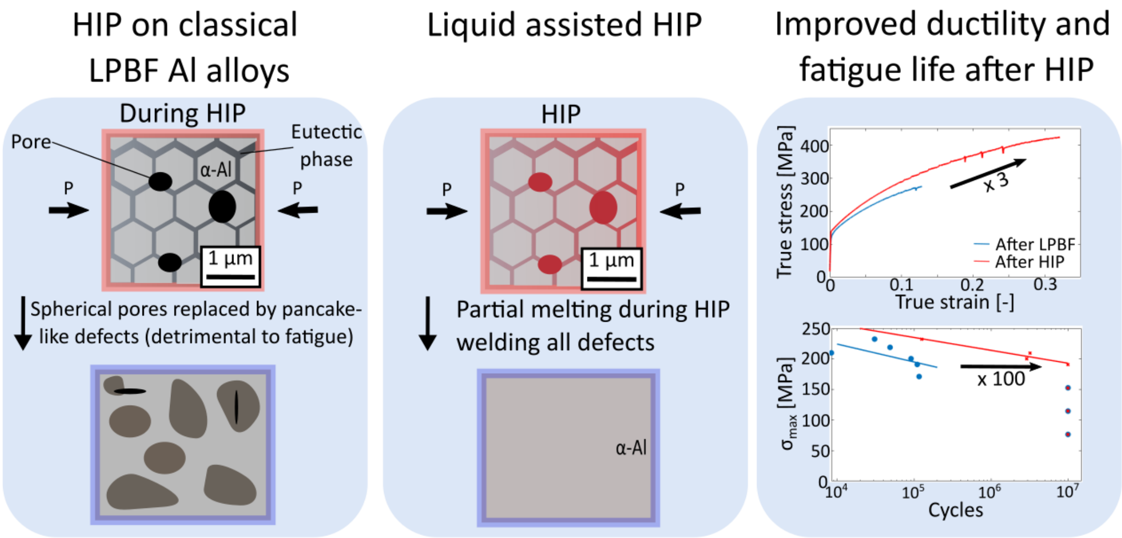

Main

One of the most developed additive manufacturing technologies for metallic materials is Laser Powder Bed Fusion (LPBF), also called Selective Laser Melting (SLM). [1] For transportation industries, Al alloys are attractive due to their excellent strength to weight ratio leading to fuel savings. [2] Researches have focused first on Al-Si alloys due to their excellent castability, and thus, suitability for LPBF [2] and then, on high strength LPBF Al alloys such as 7xxx series Al alloys. [3] However, one of the main issues of these 7xxx series Al alloys is their hot cracking susceptibility and the porosity level in the part. [4] Such defects are known to have a detrimental influence on fatigue life due to early fatigue crack nucleation. [5] This still hinders the difficult introduction of new LPBF Al alloys on the high-end applications market, which requires high reliability, i.e. high density, mechanical properties and resistance to fatigue loading.

In order to overcome these issues, different approaches are developed such as the optimization of the LPBF parameters, which can reduce up to a certain level the porosity. [6] However, this is not always sufficient to fulfil the requirements of high-end applications. Therefore, a common solution consists in a post-processing step: Hot Isostatic Pressing (HIP). The part is subjected to a heat treatment under hydrostatic pressure in an inert atmosphere. [7]

This is expected to compress the part in order to close the voids and thus, increase the density and delay fatigue crack nucleation. Although HIP has shown promising results as post-treatment on steel [8], nickel [9] and titanium [10-13] alloys, it is detrimental for Al alloys. [14-16] In literature, different HIP treatments from 330 °C to 530 °C were investigated with pressures from 100 MPa to 300 MPa on AlSi10Mg. [15, 17] Note that all these temperatures lie below the solidus of the alloy meaning that no liquid phase was present during these HIP treatments. Santos Macias *et al.* selected 300 MPa as a promising pressure for HIP as it significantly reduced the porosity and increased the fracture strain [16] while a pressure of 100 MPa was insufficient to completely remove the pores. [17] However, even at that pressure, HIP does not fully weld the porosities but flattens them (i.e. seals them), meaning that some pores are replaced by pancake-like defects or cracks (see **Figure 1a, b** and **c**). [15, 16] This induces a larger stress concentration at the tip of the defects compared to the initial spherical porosity and thus, premature failure. Moreover, some pores reopening was also reported due to the high gas pressure initially present in the porosities. [18, 19] Finally, the increased HIP temperature induces a decrease of the yield strength caused by a coarsening of the microstructure. All these phenomena lead to an alloy with a lower fatigue strength after HIP treatment. [17]

In this paper, liquid assisted healing is applied during HIP treatment on a new class of Al alloys, especially tailored for effective HIP, see **Figure 1a**, **d** and **e**. The concept consists in selecting a HIP temperature in the mushy zone of the alloy (see above 450 °C for Al-Mg alloys, in blue area on **Figure 1f**) in order to induce partial melting and thus, completely heal the defects (see **Figure 1a**, **d** and **e**) instead of only allowing diffusion during the HIP treatment, which is not enough as observed in classical LPBF Al alloys (see **Figure 1a**, **b** and **c**). Al alloys presenting a large temperature range where liquid and solid coexist (between solidus and liquidus temperatures) are thus required. Indeed, only part of the material should melt to keep the structural integrity of the part. After manufacturing of these alloys by LPBF, they present

LPBF pores in a microstructure composed of α-Al cells surrounded by a eutectic phase E (see **Figure 1a**). Note that this eutectic phase takes the shape of a network due to the high cooling rate of LPBF. [20] A HIP treatment at a temperature triggering partial melting of the alloy (in the mushy zone) is thus applied (see **Figure 1f** and **g**). Approximately 15 % of liquid fraction is targeted here in order to mimic liquid sintering where densification is also achieved due to solid grains coexisting with a liquid phase. [21] This liquid flows in the pores and welds them during solidification (see **Figure 1d**). The rest of the alloy remains in solid state in order to maintain structural integrity. After HIP, the microstructure had time to reach the stable full FCC α-Al phase without eutectic (see **Figure 1e**).

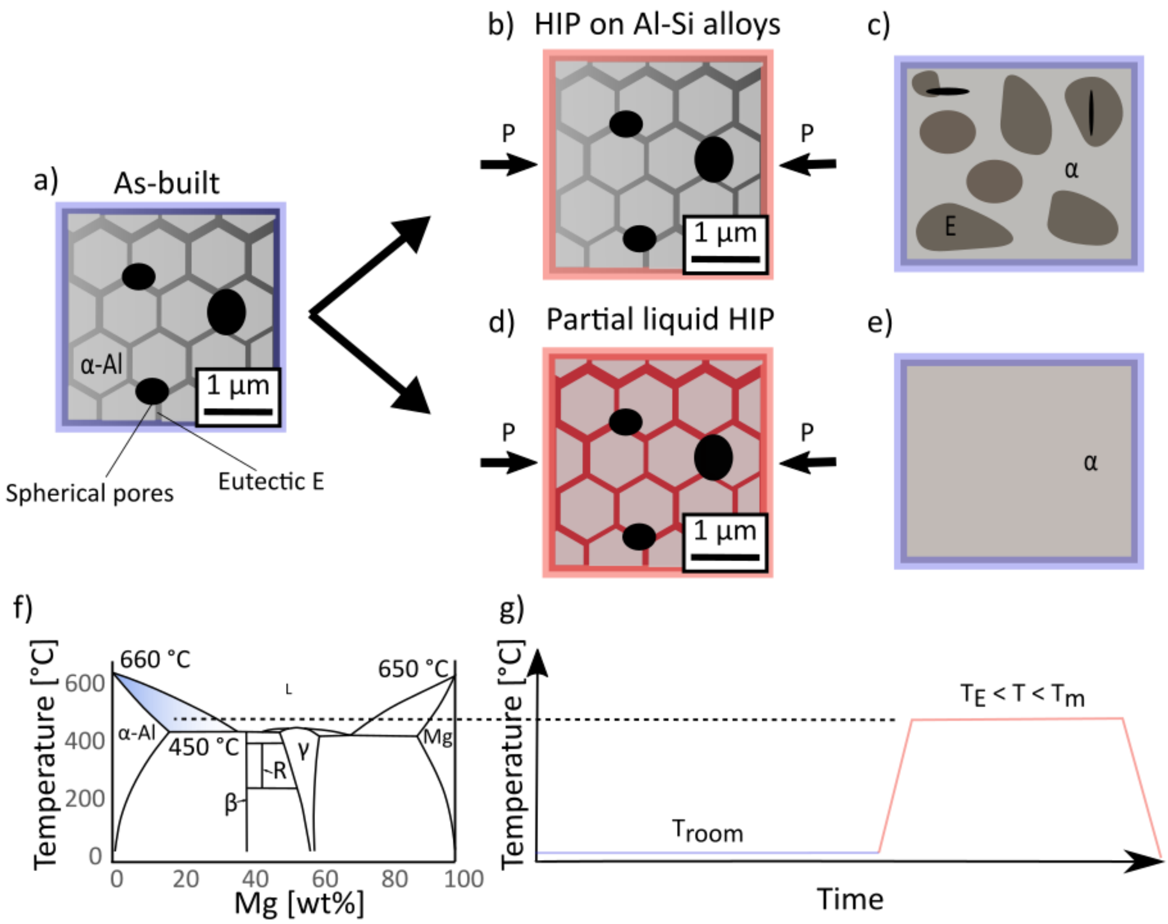

Figure 1. Schematic of the microstructure of commercial LPBF Al alloys (a,b,c) and the new class of Al alloys tailored for HIP (a,d,e) in as-built state (a), during HIP (b,d) and after HIP (c,e). The α-Al phase, solid eutectic network phase E, melted eutectic network phase E and LPBF porosities are depicted in light grey, dark grey, red and black, respectively. Blue and red boxes represent room temperature and HIP temperature conditions, respectively. f) Binary phase diagram of Al-Mg system studied in this paper and g) Temperature profile during HIP.

Binary Al-Mg alloys are materials of choice for this proof-of-concept because of their low solidus temperature and large solidification range (see **Figure 1f**). In order to obtain a fully FCC microstructure after HIP and to minimize the solidus temperature (to minimize the HIP temperature), a composition of 14 wt% Mg is selected as it is below the solubility limit of Mg (15 wt% at 450°C, see **Figure 1f**).

The Al-Mg composition studied in this work was obtained by mixing 99.7 wt% pure Al (from 3D Systems) with 99.8 wt% pure Mg (from SFM) in a Turbula powder blender. Powder mixing was performed for at least two hours. The obtained chemical composition was Al (balance), Mg (13.7 ± 0.1 wt%), Si (0.05 ± 0.01 wt%) and Fe (0.1 ± 0.01 wt%). The particle size distribution of the powder mix varies from 14.3 µm to 57.8 µm with a mean value of 35.5 µm. The samples were manufactured by LPBF on a ProX200 machine from 3D Systems under an argon inert atmosphere with an oxygen content below 500 ppm. The LPBF parameters were optimized using the methodology developed by Gheysen *et al.* [6] : laser power of 216 W, scanning speed of 500 mm s^{-1}, hatching space of 75 µm and layer thickness of 30 µm. Due to evaporation of Mg during the process, the final composition of the manufactured parts, obtained by inductively coupled plasma optical emission spectroscopy, is Al – 8.4 wt% Mg called AlMg8.4.

Hot isostatic pressing (HIP) was performed at the "CARAMEL" platform facility of Université Sorbonne Paris Nord (USPN). An Argon isostatic pressure of 300 MPa (as suggested by Santos *et al.* [16]) with a temperature of 540 °C for 30 minutes were selected in order to obtain 15 % of liquid fraction based on differential scanning calorimetry (see in **Figure S1** in supplementary materials and Ref. [22]). The heating and cooling rates were 10 °C min^{-1}.

Multi-scale X-ray nano-holo-tomography experiments (nano-CT) with a voxel size of 35 nm or 200 nm were performed on beamline ID16B at the ESRF synchrotron (Grenoble, France). [23] The samples were polished to reach a thickness of 300 µm and then cut using a micro-cutting machine. They were mounted on an alumina tube using cement glue (to resist high temperatures) and this alumina tube was fixed on a brass holder in order to be placed on the beam path (see the set-up in **Figure S2** in supplementary materials). The samples were first scanned at ESRF, then HIP treated and scanned again at ESRF to follow the porosity evolution. The scans were then reconstructed, registered and segmented using the Avizo software.

Uniaxial tensile tests were performed using a Deben 5kN microtensile machine at a strain rate of about 0.001 mm s^{-1}. Digital image correlation (camera Allied Vision Manta G-1236B POE (12 MPix)) was used to record the true local strain. Plates were manufactured by LPBF and then electrical discharge machined to obtain the required geometry, i.e. thickness, reduced section length and width are 1.5 mm, 4 mm and 2 mm, respectively (see all dimensions in **Figure S3** in supplementary materials).

Fatigue tests were performed to investigate the influence of HIP on the total fatigue life. Cylinders were manufactured by LPBF and then milled to obtain the geometry according to ASTM E466-15, i.e. diameter of the minimum cross section and radius of curvature are 2 mm and 40 mm, respectively (see all dimensions in **Figure S3** in supplementary materials). Samples were then polished up to a roughness *Ra* < 0.25 µm. The tests were performed on a 25 kN MTS Bionix servohydraulic machine following the ASTM E466-15 standard. The fatigue test is force controlled constant amplitude axial tensile-tensile with a *R* ratio of 0.1 and a frequency of 30 Hz.

First, the efficiency of HIP to seal LPBF pores in AlMg8.4 is assessed using X-ray nano-CT at European Synchrotron Radiation Facility (ESRF) on the exact same location before and after HIP (see **Figure 2**). The sealing of almost all of the pores during HIP is clearly evidenced on **Figure 2(a-d)** even looking at the one of approximately 80 µm. It means that 300 MPa is indeed an adequate pressure to seal the porosities by creep and plastic deformation, even the largest ones. However, the voxel size of 200 nm does not allow to see if the pores were completely healed or became pancake-like defects as reported by Finfrock *et al.*. [15] Thus, **Figure 2e** and **f** show the porosity before and after HIP in a sub-volume acquired at a higher resolution, i.e. 35 nm. Even at this scale, the vast majority of pores seem again closed and no pancake-like defect are observed. Very small pores seem to remain but will sure not be critical as they represent 0.008 % in volume. This is much lower than in common wrought Al alloys (e.g. 0.037 % in 6056 alloy [24]). The HIP treatment seems promising to completely heal the inner pores. Indeed, looking at the surface of the sample (see **Figure 2b**), open pores remain after HIP as expected due to the highly pressurized gas. [25] Note that sand blasting or vibratory finishing are commonly performed on LPBF parts to minimize their roughness. [26] These open porosities are thus expected to be suppressed during this post-treatment and should therefore not be detrimental to the fatigue life.

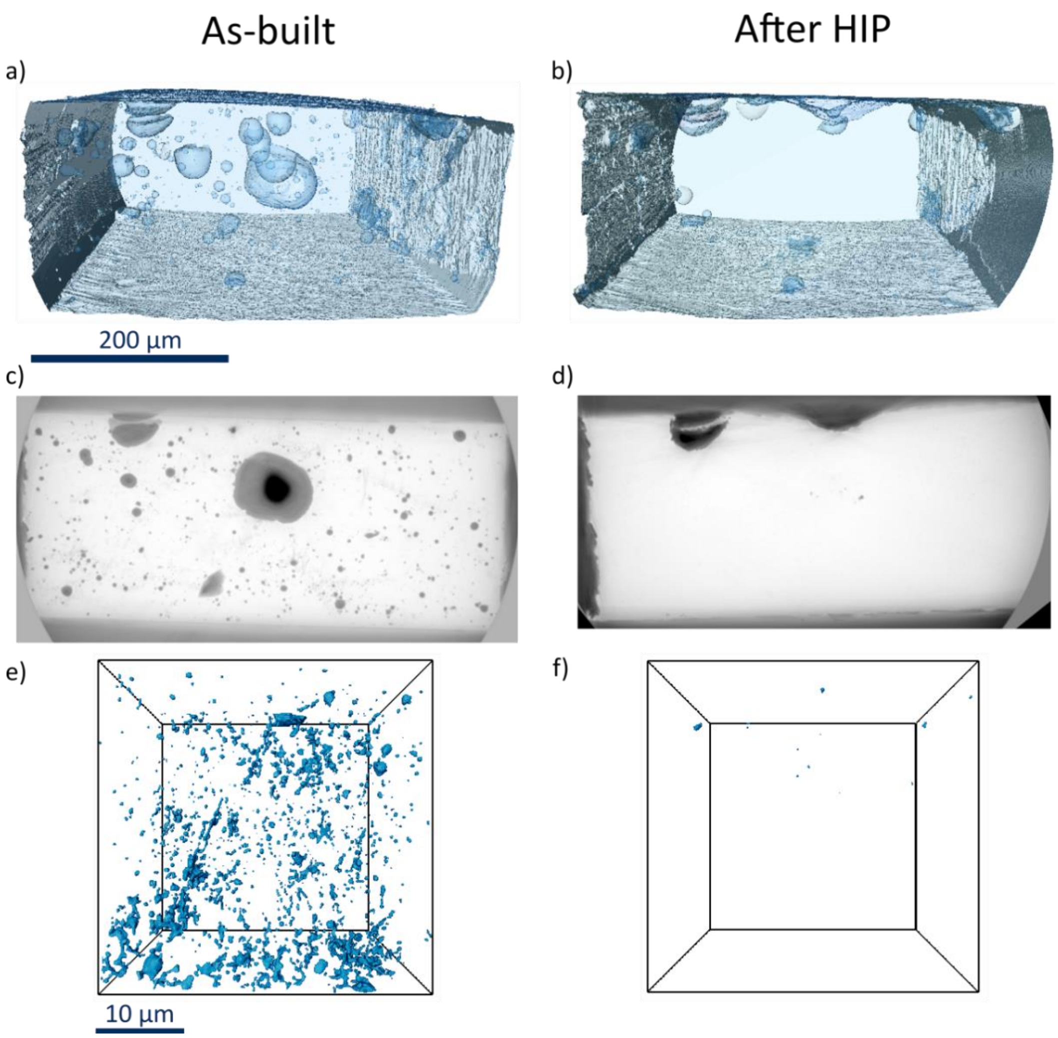

Figure 2. Reconstructed volume of the full sample obtained by X-ray nano-CT a) before and b) after HIP post-treatment with a voxel size of 200 nm. Minimum intensity projection along z for the first 44 µm of the reconstructed volumes presented above c) before and d) after HIP. 3D rendering of the voids (in blue) within a chosen sub-volume ROI of the sample with a voxel

size of 35 nm e) before and f) after HIP. Only the voids with a size larger than 3 voxels are represented.

Finally, distortion and shrinkage of the part are observed (see **Figure 2b**) after HIP. This is a common issue of HIP observed for all materials. In this case, this slight distortion is probably the result of the closing of the large pores such as the one of 80 µm diameter in the middle of the part. This is not the scope here but if a highly accurate part is required, the distortion can be taken into account during the design of the LPBF part for example based on finite element simulation [27, 28] or neural network approach. [29]

Figure 3 shows the microstructure of AlMg8.4 before and after HIP. As expected (see **Figure 1a**), α-Al cells are surrounded by a eutectic network in the as-built (AB) state (see **Figure 3a).** After HIP, the microstructure became the stable (see **Figure 1f**) full α-Al grains (see **Figure 3b**). During the HIP treatment, a coarsening of the grain size from 6.6 ± 1.3 µm to 16.8 ± 8.1 µm is observed using the line intercept method on more than 50 grains.

Figure 4a shows the tensile properties of AlMg8.4 before and after HIP. The HIP treatment induces a slight increase of the yield strength (from 132 ± 2 MPa to 139 ± 7 MPa) and an exceptional increase of the elongation at failure (from 12 ± 3 % to 33 ± 1 %). This significant improvement of the fracture strain is expectedly due to the welding of the pores during HIP but also to the completely different microstructure which is only composed of α-Al grains without any brittle eutectic network after HIP (see **Figure 3b**). [30] The disappearance of the pores and this brittle eutectic network induces a clear decrease of the damage nucleation sites in the alloy which is expected to be the cause of the increased ductility. All the Mg is thus present in solid solution in the α-Al phase which induces a slight increase in strength of the alloy. The combination of all these phenomena significantly improves the tensile properties of the new AlMg8.4 especially tailored for HIP post-treatment.

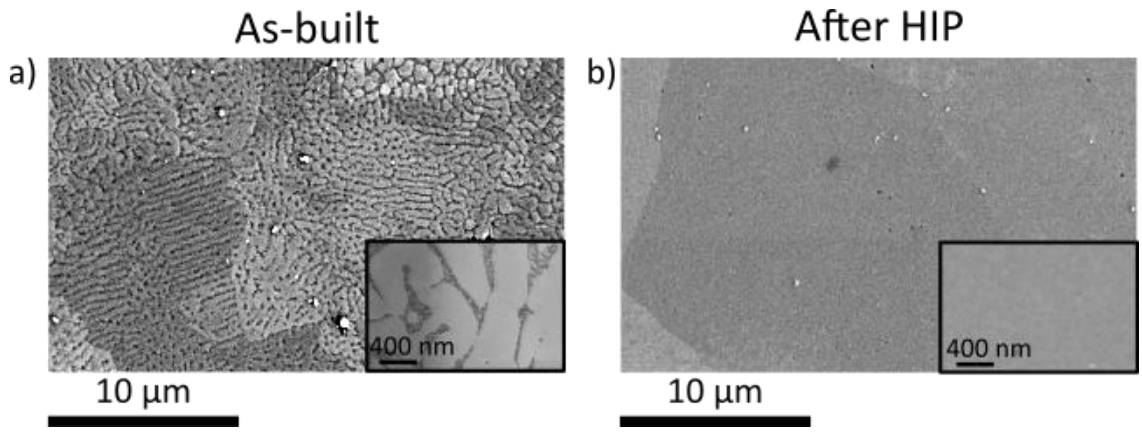

Figure 3. SEM images of the microstructure of AlMg8.4 a) before and b) after HIP treatment. Insets are higher magnification observations of the microstructure.

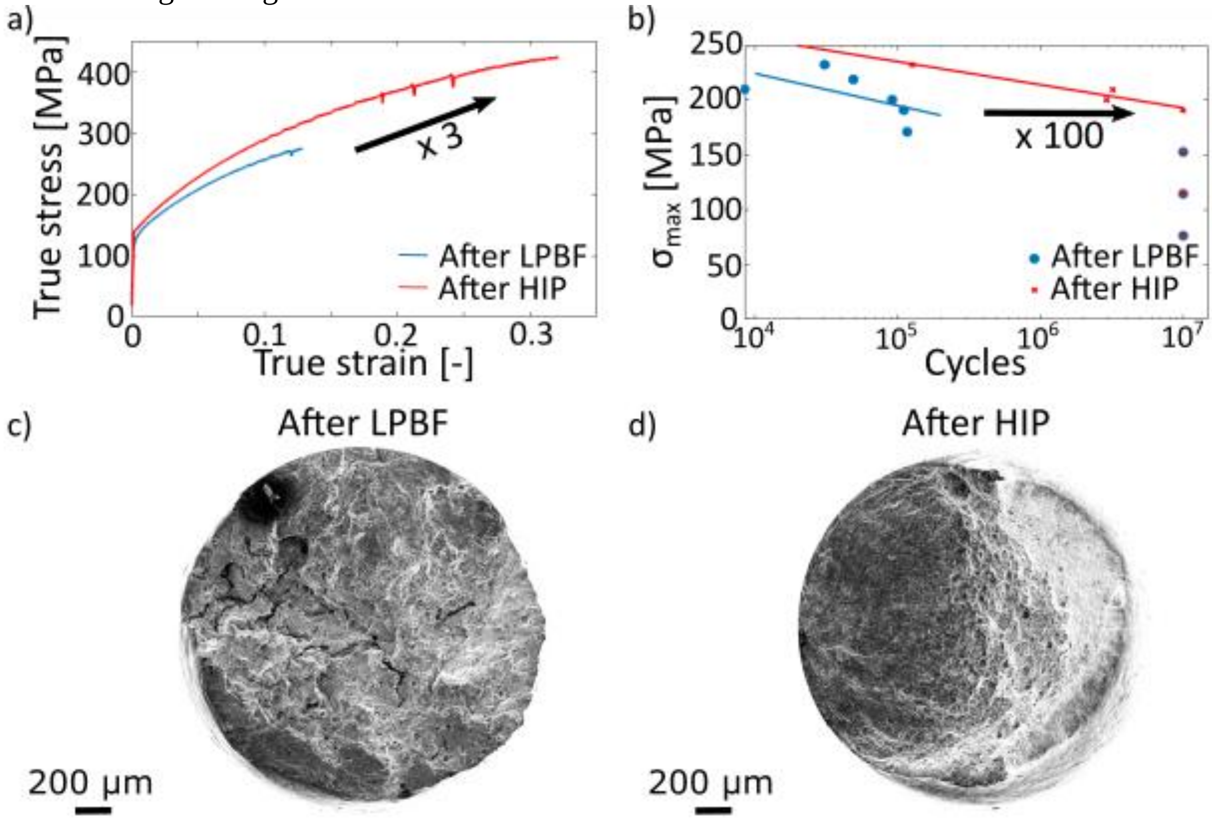

Figure 4. a) Representative true tensile curves of AlMg8.4 in as-built (AB) state (in blue) and after HIP (in red). b) Wöhler curve of LPBF AlMg8.4 under AB (blue) and HIP (red) conditions. The arrowed points represent samples that did not break after 10^7 cycles. The straight lines correspond to Basquin's law fitting of the broken samples data (see **Equation S1** and **Table S1** in supplementary materials). SEM images of the fracture surface of the fatigue specimen corresponding to σ_{max} of 175 MPA after c) LPBF and d) HIP.

Finally, the total fatigue life (Wöhler curve) of AlMg8.4 with and without HIP treatment can be observed on **Figure 4b**. Up to a maximum stress of 150 MPa (higher than the yield strength of 132 MPa), none of the AB and HIPed samples break even after 10^7 cycles. Above the maximal stress of 150 MPa, the HIPed samples exhibit a significantly improved fatigue life compared to the AB alloy. Indeed, HIP induces a huge increase of a factor 100 of the fatigue life for a σ_{max} equal to 1.25 σ_Y. This is attributed to the complete welding of the LPBF porosities during HIP due to partial melting of the alloy combined with a slightly increased yield strength during HIP. The fracture surface of the fatigue specimen tested to obtain the Wöhler curves were observed by SEM on **Figure 4c and d**. In both cases, the crack responsible of the fracture initiated at the surface of the sample. However, in the as-lpbf sample, different other cracks initiated due to the presence of defects. In the HIPed, no clear defect could be identified and a ductile fracture is noticed. Porosity does not reopen during fatigue loading contrarily to what is observed for conventional HIPed LPBF Al alloys. [18, 19]

In conclusion, a new class of LPBF Al alloys inspired from liquid-state healing strategies were especially designed for the HIP treatment. A healing temperature selected in the mushy zone induces partial melting of the alloys during HIP and thus, a complete healing of almost all the LPBF porosities is expected. This leads to an exceptional increase of the tensile properties, in particular, the fracture strain of the alloy is almost tripled, as well as a substantial increased fatigue life up to a factor 100. This liquid assisted healing HIP treatment of the alloy is expected to be translatable to other Al alloys presenting a large solidification range but possibly exhibiting a higher yield strength. A temperature triggering 15 % of liquid fraction was selected. This liquid assisted healing HIP treatment might also be interesting not as a post-treatment but as healing treatment in order to repair the part after an overload.

Acknowledgements

We acknowledge the European Synchrotron Radiation Facility for provision of synchrotron radiation facilities (experiment MA4874 and inhouse beamtime) and we would like to thank Florent Hannard, Grzegorz Pyka and Mariia Arseenko for assistance in using beamline ID16b. J.G. is supported by the Fonds de la recherche scientifique – FNRS (FRIA grant), Belgium. J.G. and A.S are funded by the European Research Council (ERC) (grant agreement n°716678). We acknowledge the European Synchrotron Radiation Facility for provision of synchrotron radiation facilities (proposal MA4874). We acknowledge the Université Sorbonne Paris Nord (USPN) “CARAMEL” platform facility funded by Région Île-de-France and the CNRS for the HIP post-treatments. Avizo software acquisition was supported by the Fonds de la Recherche Scientifique – FNRS - EQP under grant UN06920F. We acknowledge Sophie De Raedemacker for the SEM images of the fracture surfaces.

References

[1] M. Nematollahi, A. Jahadakbar, M.J. Mahtabi, M. Elahinia, 12 - Additive manufacturing (AM), in: M. Niinomi (Ed.), Metals for Biomedical Devices (Second Edition), Woodhead Publishing2019, pp. 331-353.
[2] N. Kang, P. Coddet, C. Chen, Y. Wang, H. Liao, C. Coddet, Microstructure and wear behavior of in-situ hypereutectic Al–high Si alloys produced by selective laser melting, Materials & Design 99 (2016) 120-126.
[3] J.e. Sun, B. Zhang, X. Qu, High strength Al alloy development for laser powder bed fusion, Journal of Micromechanics and Molecular Physics 06(02) (2021) 2141001.
[4] Y. Cao, H.L. Wei, T. Yang, T.T. Liu, W.H. Liao, Printability assessment with porosity and solidification cracking susceptibilities for a high strength aluminum alloy during laser powder bed fusion, Additive Manufacturing 46 (2021) 102103.
[5] J.G. Santos Macías, C. Elangeswaran, L. Zhao, B. Van Hooreweder, J. Adrien, E. Maire, J.-Y. Buffière, W. Ludwig, P.J. Jacques, A. Simar, Ductilisation and fatigue life enhancement of selective laser melted AlSi10Mg by friction stir processing, Scripta Materialia 170 (2019) 124-128.
[6] J. Gheysen, M. Marteleur, C. van der Rest, A. Simar, Efficient optimization methodology for laser powder bed fusion parameters to manufacture dense and mechanically sound parts validated on AlSi12 alloy, Materials & Design 199 (2021) 109433.
[7] P. Li, D.H. Warner, J.W. Pegues, M.D. Roach, N. Shamsaei, N. Phan, Investigation of the mechanisms by which hot isostatic pressing improves the fatigue performance of powder bed fused Ti-6Al-4V, International Journal of Fatigue 120 (2019) 342-352.
[8] A. Röttger, K. Geenen, M. Windmann, F. Binner, W. Theisen, Comparison of microstructure and mechanical properties of 316L austenitic steel processed by selective laser melting with hot-isostatic pressed and cast material, Materials Science and Engineering: A 678 (2016) 365-376.
[9] A. Kreitcberg, V. Brailovski, S. Turenne, Effect of heat treatment and hot isostatic pressing on the microstructure and mechanical properties of Inconel 625 alloy processed by laser powder bed fusion, Materials Science and Engineering: A 689 (2017) 1-10.
[10] S. Leuders, M. Thöne, A. Riemer, T. Niendorf, T. Tröster, H.A. Richard, H.J. Maier, On the mechanical behaviour of titanium alloy TiAl6V4 manufactured by selective laser melting: Fatigue resistance and crack growth performance, International Journal of Fatigue 48 (2013) 300-307.
[11] M.-W. Wu, J.-K. Chen, B.-H. Lin, P.-H. Chiang, Improved fatigue endurance ratio of additive manufactured Ti-6Al-4V lattice by hot isostatic pressing, Materials & Design 134 (2017) 163-170.
[12] M.-W. Wu, P.-H. Lai, The positive effect of hot isostatic pressing on improving the anisotropies of bending and impact properties in selective laser melted Ti-6Al-4V alloy, Materials Science and Engineering: A 658 (2016) 429-438.

[13] T. Mishurova, K. Artzt, B. Rehmer, J. Haubrich, L. Ávila, F. Schoenstein, I. Serrano-Munoz, G. Requena, G. Bruno, Separation of the impact of residual stress and microstructure on the fatigue performance of LPBF Ti-6Al-4V at elevated temperature, International Journal of Fatigue 148 (2021) 106239.
[14] N.O. Larrosa, W. Wang, N. Read, M.H. Loretto, C. Evans, J. Carr, U. Tradowsky, M.M. Attallah, P.J. Withers, Linking microstructure and processing defects to mechanical properties of selectively laser melted AlSi10Mg alloy, Theoretical and Applied Fracture Mechanics 98 (2018) 123-133.
[15] C.B. Finfrock, A. Exil, J.D. Carroll, L. Deibler, Effect of Hot Isostatic Pressing and Powder Feedstock on Porosity, Microstructure, and Mechanical Properties of Selective Laser Melted AlSi10Mg, Metallography, Microstructure, and Analysis 7(4) (2018) 443-456.
[16] J.G. Santos Macías, L. Zhao, D. Tingaud, B. Bacroix, G. Pyka, C. van der Rest, L. Ryelandt, A. Simar, Hot isostatic pressing of laser powder bed fusion AlSi10Mg: parameter identification and mechanical properties, Journal of Materials Science 57(21) (2022) 9726-9740.
[17] I. Rosenthal, E. Tiferet, M. Ganor, A. Stern, Post-processing of AM-SLM AlSi10Mg specimens: Mechanical properties and fracture behaviour, Annals of "Dunarea de Jos" University of Galati. Fascicle XII, Welding Equipment and Technology 26 (2015) 33-38.
[18] J.C. Hastie, M.E. Kartal, L.N. Carter, M.M. Attallah, D.M. Mulvihill, Classifying shape of internal pores within AlSi10Mg alloy manufactured by laser powder bed fusion using 3D X-ray micro computed tomography: Influence of processing parameters and heat treatment, Materials Characterization 163 (2020) 110225.
[19] J.C. Hastie, J. Koelblin, M.E. Kartal, M.M. Attallah, R. Martinez, Evolution of internal pores within AlSi10Mg manufactured by laser powder bed fusion under tension: As-built and heat treated conditions, Materials & Design 204 (2021) 109645.
[20] Y.L. Liu, S.B. Kang, Solidification and segregation of Al-Mg alloys and influence of alloy compositionand cooling rate, Materials Science and Technology 13(4) (1997) 331-336.
[21] R.M. German, Chapter Nine - Sintering With a Liquid Phase, in: R.M. German (Ed.), Sintering: from Empirical Observations to Scientific Principles, Butterworth-Heinemann, Boston, 2014, pp. 247-303.
[22] J. Gheysen, Design, development and characterisation of new healable laser powder bed fusion aluminium alloys, Université Catholique de Louvain, Université Catholique de Louvain, 2022.
[23] J. Gheysen, M. Arseenko, F. Hannard, E. Maire, G. Pyka, A. Simar, J. Villanova, Investigation by 3D nano-holotomography of the self-healability of an Aluminium alloy produced by additive manufacturing, in: E.S.R. Facility (Ed.) 2021.
[24] F. Hannard, S. Castin, E. Maire, R. Mokso, T. Pardoen, A. Simar, Ductilization of aluminium alloy 6056 by friction stir processing, Acta Materialia 130 (2017) 121-136.
[25] B.J. Kellett, F.F. Lange, Experiments on Pore Closure During Hot Isostatic Pressing and Forging, Journal of the American Ceramic Society 71(1) (1988) 7-12.
[26] E. Maleki, S. Bagherifard, M. Bandini, M. Guagliano, Surface post-treatments for metal additive manufacturing: Progress, challenges, and opportunities, Additive Manufacturing 37 (2021) 101619.
[27] A. Du Plessis, B. Yelamanchi, C. Fischer, J. Miller, C. Beamer, K. Rogers, P. Cortes, J. Els, E. MacDonald, Productivity enhancement of laser powder bed fusion using compensated shelled geometries and hot isostatic pressing, Advances in Industrial and Manufacturing Engineering 2 (2021) 100031.
[28] W.X. Yuan, J. Mei, V. Samarov, D. Seliverstov, X. Wu, Computer modelling and tooling design for near net shaped components using hot isostatic pressing, Journal of Materials Processing Technology 182(1) (2007) 39-49.

[29] O. Dengiz, A. Konak, S. Kulturel-Konak, A.E. Smith, I. Nettleship, Neural Computing Approach to Shape Change Estimation in Hot Isostatic Pressing, in: I.C. Parmee (Ed.) Adaptive Computing in Design and Manufacture V, Springer London, London, 2002, pp. 171-180.
[30] L. Zhao, J.G. Santos Macías, L. Ding, H. Idrissi, A. Simar, Damage mechanisms in selective laser melted AlSi10Mg under as built and different post-treatment conditions, Materials Science and Engineering: A 764 (2019) 138210.

Supporting Information

Exceptional Fatigue Life and ductility of New Liquid Healing Hot Isostatic Pressing Especially Tailored for Additive Manufactured Aluminum Alloys

Julie Gheysen, David Tingaud, Julie Villanova, Azziz Hocini and Aude Simar*

Equation S1. The Basquin's fitting law

$$\Delta\sigma = C \cdot N_f^b \tag{1}$$

where $\Delta\sigma = \sigma_{max} - \sigma_{min}$, N_f = Number of cycles to failure and b and C [MPa] are material constants, provided in **Table S1**.

	After LPBF	After HIP
C [MPa]	1.44	0.35
b	-0.19	-0.04

Table S1. Basquin fitting parameters C [MPa] and b after LPBF and after HIP treatment.

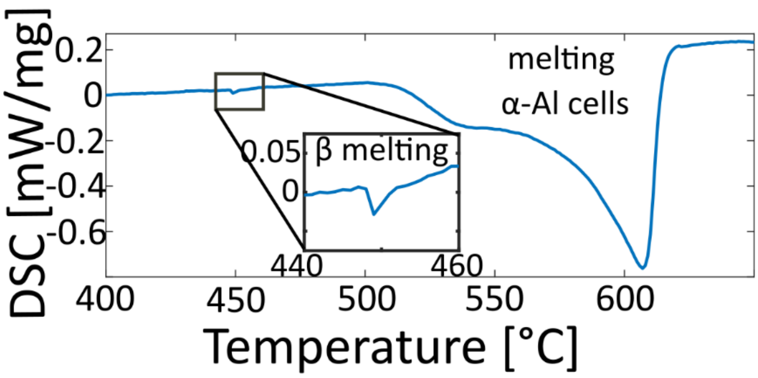

Figure S1. Differential scanning calorimetry heating curve at 10 °C/min up to 660 °C of AlMg8.4.

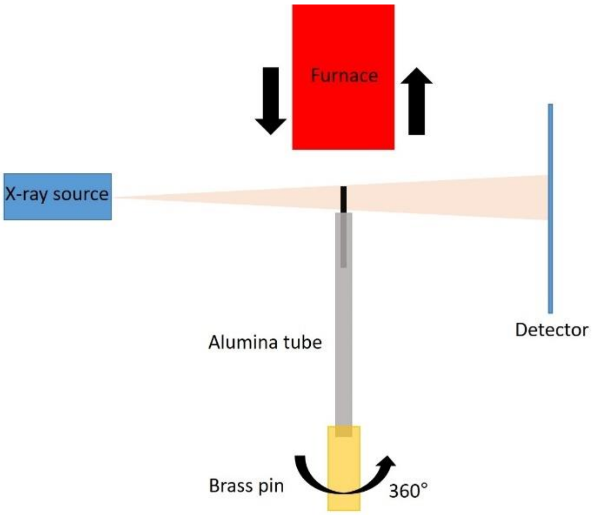

Figure S2. Schematic representation of the 3D X-ray nano-holo-tomography set-up.

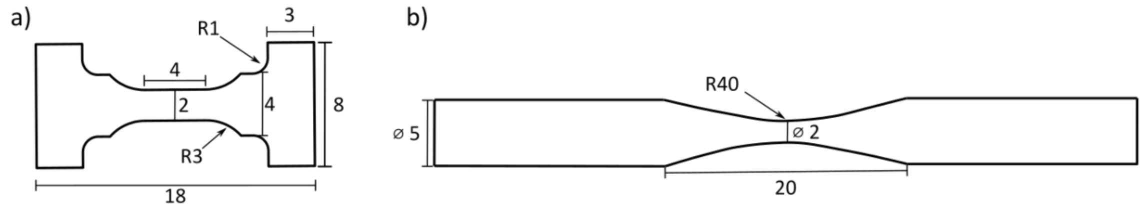

Figure S3. Geometry of a) the microtensile samples and b) the fatigue samples.